Title

Explaining the Size Dependence in Platinum-Nanoparticle-Catalyzed Hydrogenation Reactions

Journal

Angewandte Chemie International Edition, 55(50)

ISSN

1433-7851

Authors

Bai, Licheng
Wang, Xin
Chen, Qiang
et al.

Publication Date

2016-12-12

DOI

10.1002/anie.201609663

Peer reviewed

Nanoparticle Catalysts Hot Paper

International Edition: DOI: 10.1002/anie.201609663
German Edition: DOI: 10.1002/ange.201609663

Explaining the Size Dependence in Platinum-Nanoparticle-Catalyzed Hydrogenation Reactions

Licheng Bai, Xin Wang, Qiang Chen, Yifan Ye, Haoquan Zheng, Jinghua Guo, Yadong Yin,* and Chuanbo Gao**

Abstract: *Hydrogenation reactions are industrially important reactions that typically require unfavorably high H_2 pressure and temperature for many functional groups. Herein we reveal surprisingly strong size-dependent activity of Pt nanoparticles (PtNPs) in catalyzing this reaction. Based on unambiguous spectral analyses, the size effect has been rationalized by the size-dependent d-band electron structure of the PtNPs. This understanding enables production of a catalyst with size of 1.2 nm, which shows a sixfold increase in turnover frequency and 28-fold increase in mass activity in the regioselective hydrogenation of quinoline, compared with PtNPs of 5.3 nm, allowing the reaction to proceed under ambient conditions with unprecedentedly high reaction rates. The size effect and the synthesis strategy developed herein may provide a general methodology in the design of metal-nanoparticle-based catalysts for a broad range of organic syntheses.*

Metal nanoparticles have emerged as a new platform for developing highly efficient catalysts in view of their tunable size, morphology, and composition.[1–14] However, substantial challenges still remain when these nanoparticles are used as the catalyst for many organic syntheses. These challenges include that the systematic relationship between the properties of metal nanoparticles and their catalytic performance is yet to be fully established, and that the stabilization and precise size engineering of these catalysts are difficult, especially of ultrasmall one.[15–19] In a more specific scenario, supported Pt nanoparticles (PtNPs) are promising candidates for various hydrogenation reactions. However, many synthetic PtNPs show low catalytic activity in hydrogenation of certain functionalities and undesired selectivity when dealing with multifunctional molecules.[20,21] In the regioselective hydrogenation of quinoline with hydrogen, which is important for the synthesis of many biologically active molecules,[22] both homo- and heterogeneous catalytic systems have been developed including transition-metal complexes[23–26] and nanoparticles.[20,21,27,28] However, they usually require very harsh conditions, for example, a high hydrogen pressure (1–4 MPa) or an elevated temperature (40–200 °C), which may cause high cost and potential safety concerns in practical operations. Although there have been few reports of catalysts that allow the regioselective hydrogenation of quinoline and its derivatives under relatively mild conditions,[23,28] it remains a challenge to fully manipulate the properties and performance of the catalysts to give optimal catalytic systems.

The harsh condition required for the hydrogenation reactions suggests that the strength of the interaction between the PtNPs and the reactants is too weak. Herein, based on the resin-stabilized ultrasmall PtNPs, we reveal that the size of the PtNPs has a critical influence on their bonding strength with both hydrogen and quinoline molecules. As a result, we were able to observe volcanoshaped dependence of the catalytic activity on the size of the PtNPs, with those of approximately 1.2 nm exhibiting record-high activity in hydrogenation of quinoline. Although the influence of the nanoparticle size has been observed in hydrogenation reactions with Pt catalyst in the literature, it should be noted that many reports relied on catalysts with wide ranges of particle sizes that introduce ambiguity, the demonstrated size effect was mostly focused on the reaction selectivity, and the mechanism of the size effect remained less-well understood.[29–34] Herein, we observe surprisingly strong effect of the particle size in the range of 0.7–5.3 nm on the activity of the hydrogenation reactions. With unambiguous spectral support, the size effect has been attributed to the shift of the d-band center with reference to the valence band maximum (VBM). Our strategy enables the systematic tuning of the metal-nanoparticle-based catalysts to give exceptional catalytic activities.

Effective stabilization and precise size control of the PtNPs are prerequisites of the research and were achieved by coupling the chemical reduction of a Pt salt with a sol–gel

[*] L. Bai, X. Wang, Prof. C. Gao
Frontier Institute of Science and Technology, and State Key Laboratory for Mechanical Behavior of Materials
Xi'an Jiaotong University
Xi'an, Shaanxi 710054 (China)
E-mail: gaochuanbo@mail.xjtu.edu.cn

Dr. Q. Chen
School of Chemical Engineering and Technology
Xi'an Jiaotong University
Xi'an, Shaanxi 710049 (China)
E-mail: chenqiang2204@mail.xjtu.edu.cn

X. Wang, Prof. Y. Yin
Department of Chemistry
University of California, Riverside
Riverside, CA 92521 (USA)
E-mail: yadong.yin@ucr.edu

Y. Ye, Prof. J. Guo
Advanced Light Source Division, Lawrence Berkeley National Laboratory
Berkeley, CA 94720 (USA)

Dr. H. Zheng
Department of Materials and Environmental Chemistry, Stockholm University
Stockholm 10691 (Sweden)

Supporting information and the ORCID identification number(s) for the author(s) of this article can be found under http://dx.doi.org/10.1002/anie.201609663.

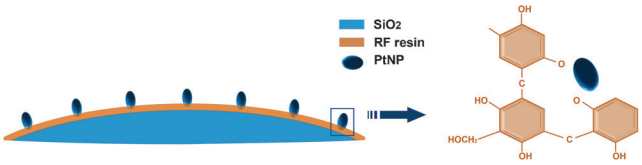

Scheme 1. Interaction between the ultrasmall PtNPs and phenolic groups of RF for the effective stabilization of the NPs.

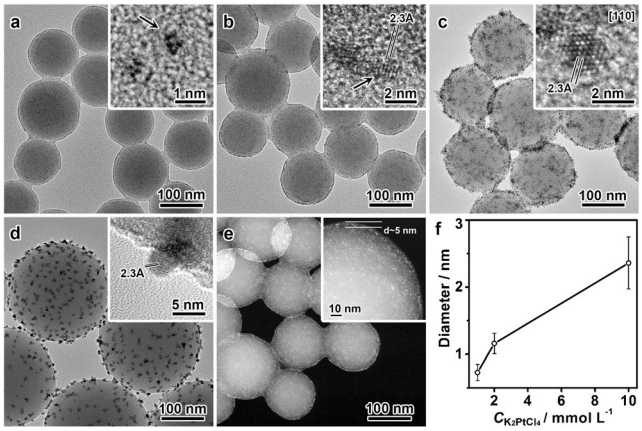

Figure 1. SiO_2@RF/Pt nanospheres with PtNPs of different sizes (Pt-*x*, *x*: diameter of the PtNPs, unit: nm). a)–d) Transmission electron microscopy (TEM) of Pt-0.7, Pt-1.2, Pt-2.4, and Pt-5.3, respectively. Inset: HRTEM of a single PtNP. Arrows indicate the PtNPs. e) HAADF-STEM of Pt-1.2. Inset: A high-magnification image. Note that PtNPs appear larger than their real size under focused electron beams of the STEM. f) A diagram showing the average size of the PtNPs as a function of the concentration of K_2PtCl_4 in the synthesis.

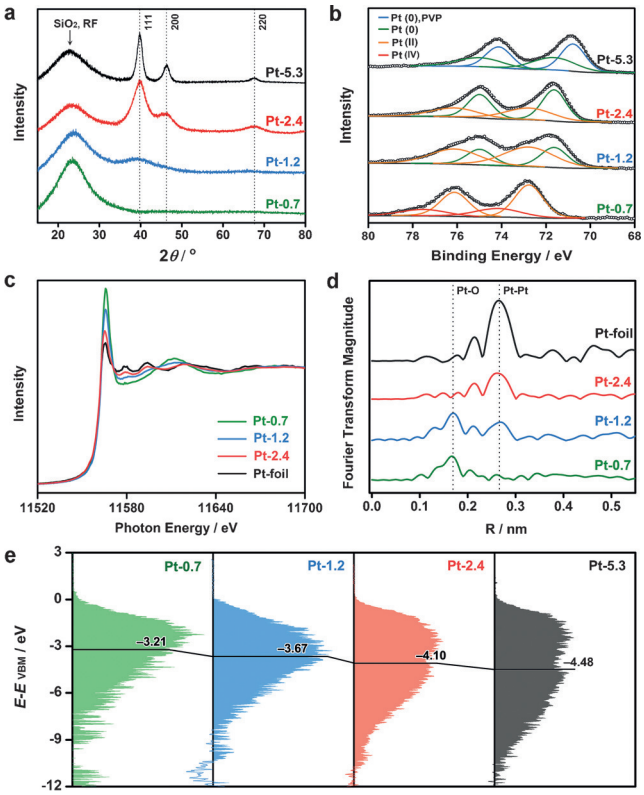

Figure 2. a),b) XRD and core-level Pt 4f XPS of Pt-*x*, where *x* = 0.7, 1.2, 2.4, and 5.3. c),d) Pt L-edge XANES (c) and FT-EXAFS spectra (d) of Pt-*x* (*x* = 0.7, 1.2, and 2.4), with Pt foil for reference. Dotted lines indicate the positions of Pt–Pt and Pt–O coordination shells. e) High-resolution valence-band Pt 5d XPS of Pt-*x* relative to the VBM, as an analogue of the density of states. Black lines indicate the positions of the d-band centers.

process of a resorcinol-formaldehyde (RF) resin (Scheme 1, Figure 1 a–c). The sol–gel process affords a thin layer of the RF resin on silica nanospheres,[35,36] which is around 5 nm in thickness revealed by high-angle annular dark-field scanning transmission electron microscopy (HAADF-STEM; Figure 1 e). The abundant phenolic groups of the RF resin provide strong multidentate interactions with the ultrasmall PtNPs formed by chemical reduction, favorable for their effective stabilization. The size of the PtNPs can be readily tuned by varying the concentration of the precursor, K_2PtCl_4 (Figure 1 f), which provides an effective means for precisely tuning their size in a range of angstroms to around 3 nm, at which size the physical properties of matter usually change dramatically. In addition, PtNPs of 5.3 nm were stabilized on amino-modified silica nanospheres to produce a control sample for systematically investigating the property and catalytic activity of the PtNPs with a broad range of sizes (Figure 1 d). These nanocatalysts are denoted as Pt-*x*, with *x* representing the average size of the PtNPs in nanometers.

Crystal structures of the PtNPs were characterized by high-resolution TEM (HRTEM; Figure 1 a–d, inset). PtNPs of large sizes (5.3 and 2.4 nm) show clear fringes of a face-centered cubic lattice. With decreasing size, the Pt lattices become less discernible at 1.2 nm while completely disappear at 0.7 nm, indicating a decrease in the crystallinity, consistent with previous observations.[10,13,37,38] The reduced crystallinity can be confirmed by the X-ray diffraction (XRD; Figure 2 a), which shows continuously broadening and eventual disappearance of the reflection peaks with decreasing size of the PtNPs.

The oxidation states of the PtNPs were analyzed by Pt 4f core-level X-ray photoelectron spectroscopy (XPS), which were fitted with spin-orbit split $4f_{7/2}$ and $4f_{5/2}$ components (Figure 2 b). PtNPs of 5.3 nm show two sets of XPS peaks, with the $4f_{7/2}$ components appearing at 71.70 and 70.80 eV of the binding energy, respectively, which can be ascribed to the bulk Pt^0 and surface Pt^0 capped with polyvinylpyrrolidone (PVP).[39] When the size of the PtNPs decreases to 2.4 and 1.2 nm, besides the XPS peaks from Pt^0, a new set of peaks emerge with $4f_{7/2}$ appearing at 72.80 eV, corresponding to Pt^{II} species. When the size of the PtNPs is down to 0.7 nm, XPS peaks from Pt^0 disappear, while the peaks from Pt^{II} are retained. Another set of peaks emerge with $4f_{7/2}$ appearing at 74.20 eV, corresponding to Pt^{IV} species. Therefore, the oxidative state of the PtNPs increases continuously with decreasing size. The oxidation state remains unchanged in a H_2 atmosphere at ambient temperature and pressure in practical catalytic reactions (Figure S5).

Pt L-edge X-ray absorption near edge structures (XANES) were analyzed to confirm the oxidation state of the nominal "PtNPs" (Figure 2c). When the size of the PtNPs decreases, the intensity of the "white lines" at 11.56 keV increases, indicating an increase in the d-band vacancy.[40] PtNPs of a large size (Pt-2.4) show fine XANES features resembling those of a Pt foil, while PtNPs of small sizes (Pt-1.2 and Pt-0.7) show fine features deviating from those of the Pt foil, with Pt-0.7 displaying similar features to those from PtO_2,[41] suggesting a gradual metal-oxide transition with decreasing size of the PtNPs. Fourier transformation of extended X-ray absorption fine structure (FT-EXAFS) further confirms the metal-oxide transition, showing weakening Pt–Pt coordination shells while emerging Pt–O shells (Figure 2d).

Therefore, a decrease of crystallinity and a metal-oxide transition were observed with the decreasing size of the PtNPs. To further reveal their interaction with hydrogen and quinoline molecules, the d-band electron structures of the PtNPs were characterized by high-resolution valence-band (VB) XPS spectra (Figure 2e), which are proportional to the density of states (DOS), and directly related to the strength of interaction between the PtNPs and guest molecules.[5,42,43] The spectra were recorded in an ultra-high vacuum (UHV), so could be different from those taken under ambient reaction conditions. Therefore, this analysis provides a general, qualitative trend of the d-band structure of the PtNPs varying with their sizes. According to the d-band center theory, when a guest molecule is adsorbed on a metal surface, hybridization between the metal d-band and an induced state by the guest molecule occurs to form fully filled bonding DOS and partially filled antibonding DOS states. The bond strength is determined by the filling degree of the antibonding states, which can be described by the position of the d-band center.[44–46] Because the antibonding states lie directly above the d electron band,[44] we chose the VBM as a reference for the d-band center.[42] Figure 2e shows a narrowing of the d electron bands with decreasing size of the PtNPs, which can be attributed to the hybridization of a lower number of the wave functions in PtNPs of a small size. It leads to a significant shift of the d-band center towards the VBM, resulting in an upward shift of the antibonding DOS states, lower occupation of them, and thus stronger interaction with guest molecules, hydrogen and quinoline in this case. On the other hand, the continuously increasing oxidation state, that is, the d-band vacancy of the PtNPs with decreasing size may also account for the stronger interaction,[14,47] owing to there being fewer electrons available for filling the antibonding DOS states.

Based on the analysis of the electron structure, as well as the prediction of increasing surface unsaturated sites, it is expected that PtNPs of appropriately small sizes may show significantly enhanced catalytic activity in regioselective hydrogenation of quinoline (Figure 3a). In a typical reaction under ambient conditions, clear differences in the catalytic activity can be observed with PtNPs of varying sizes (Figure 3b). Among them, Pt-1.2 represents the most active catalyst with conversion of quinoline reaching over 99% within 80 min, showing astonishingly high catalytic activity,

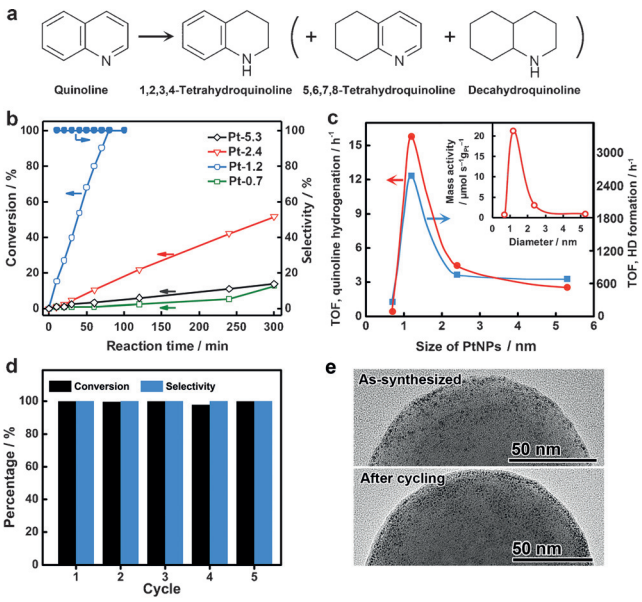

Figure 3. Catalytic activities of Pt-*x* ($x = 0.7$, 1.2, 2.4, and 5.3) in hydrogenation of quinoline at room temperature and ambient (balloon) hydrogen pressure. a) Possible products of the quinoline hydrogenation. b) Plots of conversion of quinoline and selectivity toward 1,2,3,4-tetrahydroquinoline against reaction time with Pt-*x* as the catalyst. c) Plot of TOF (per surface Pt atom) against diameter of the PtNPs. The TOF for activation of H_2 and D_2 to form HD is listed for comparison. Inset: Size-dependent mass activity (per unit mass of Pt) of the PtNPs in hydrogenation of quinoline. d) Change of conversion and selectivity in 5 cycles of the catalysis with Pt-1.2 as the catalyst. e) TEM images of the catalyst before and after cycling.

which substantially exceeds the best results in literature.[23,28] The selectivity toward 1,2,3,4-tetrahydroquinoline (THQ) was over 99% (Figure 3b). With decreasing size of the PtNPs, the turnover frequencies (TOFs) first increase and then decrease, reaching a maximum when the size of the PtNPs was 1.2 nm (Figure 3c). The champion catalyst (Pt-1.2) shows an approximately sixfold increase in the TOF compared with PtNPs of a large size, 5.3 nm, and the increase in the catalytic mass activity reaches as high as 28-fold (Figure 3c, inset). The volcano-shape profile illustrates very well the Sabatier principle,[46,48] with optimal catalytic activity achieved at a specific size of the PtNPs (ca. 1.2 nm), wherein the interaction between the PtNPs and the reactants is neither too weak (size > 1.2 nm) nor too strong (size < 1.2 nm). It is worth noting that although Pt-5.3 is capped by PVP with different surface chemistry, the size-dependence is already demonstrated based on the other three catalysts. In addition, thanks to the heterogeneous mechanism (Figure S10) and the stabilization of the ultrasmall PtNPs by the RF resin, the catalyst can be recovered from the reaction system without causing dissolution, detachment or aggregation of the PtNPs (Figure 3e, Figure S14 and Table S3 in the Supporting Information). The recovered catalyst can be repeatedly applied in the hydrogenation reactions, for example in 5 runs of our demonstration, without showing discernible decrease in the conversion of quinoline or the reaction selectivity (Figure 3d).

The size-dependent interaction between PtNPs and the reactants can be also inferred from the HD formation when flows of H_2 and D_2 are passing through the catalyst (Figure 3c). The TOF of the HD formation is size-dependent. It indicates that PtNPs of large sizes (> 1.2 nm) bind weakly to the hydrogen molecules, unfavorable for their activation, while the ultrastrong binding ability of PtNPs of small sizes (e.g., 0.7 nm) makes it difficult for the activated hydrogen to be desorbed for favorable kinetics. In addition, direct evidence for this size-dependent interaction can be obtained spectroscopically. After exposure of the catalysts to quinoline and subsequent removal of free quinoline molecules, the catalysts were subjected to ^{1}H NMR spectroscopic analysis. As shown in Figure 4a, no residual quinoline can be detected from PtNPs of large sizes (2.4 and 5.3 nm), while strong signals of quinoline were observed from PtNPs of small sizes (0.7 and 1.2 nm), confirming increasing interaction between PtNPs and quinoline with decreasing size of the PtNPs. This trend was also observed with the product, THQ, which exhibits extremely strong interaction with Pt-0.7 (Figure S13). It should be noted that the observed broadening of the ^{1}H NMR signals is consistent with previous reports on surface-bound ligands.[49] In addition, with decreasing size of the PtNPs, the ^{1}H NMR signals shift to the low fields, which suggests enhanced electron transfer from quinoline to the PtNPs, and confirms the increasing interactions. The charge transfer can be also evidenced by density function theory (DFT) calculations, with quinoline adopting a tilting configuration on the Pt surface (Figure 4b).

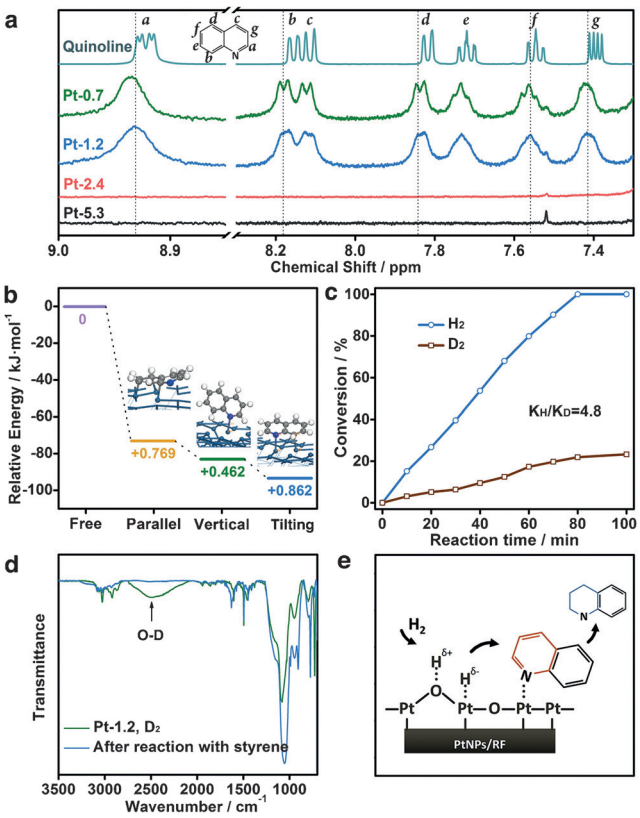

Figure 4. Catalytic mechanism of Pt-*x* in the hydrogenation of quinoline. a) ^{1}H NMR spectra of quinoline adsorbed by Pt-*x*, and that of free quinoline, suggesting different interactions between quinoline and the PtNPs. b) Adsorption modes and energies of quinoline on the Pt surface. Values under the energy levels indicate the net charges of the quinoline molecule. c) Primary isotope effect observed with Pt-1.2 in the hydrogenation of quinoline. d) The FTIR spectrum of the Pt-1.2 after exposure to D_2, showing O–D vibration. The vibration disappears after introduction of styrene. e) A proposed pathway of the hydrogenation reaction based on these results (see text for details).

The correlation between the size-dependent interaction and the activity of the catalyst was further revealed based on the understanding of the reaction mechanism. Primary isotope effect was observed with the ratio of the reaction rates (k_H/k_D) being as large as 4.8, suggesting that the rate-determining step may involve the cleavage of O–H bonds (Figure 4c).[50] As the PtNPs are composed of Pt^0 and its oxides, heterolytic dissociation of hydrogen are promoted,[51] forming O–H(δ^+) and Pt–H(δ^-) species, with the formation of O–H(δ^+) confirmed by Fourier transform infrared spectroscopy (FTIR; Figure 4d).[50] Thus, the rate-determining step can be derived to be the subsequent hydrogenation step, with hydrogen transfer from Pt–H(δ^-) and O–H(δ^+) species to the quinoline molecules. The HD formation was approximately 200-times quicker than the hydrogenation of quinoline (Figure 3c), indicating that the cleavage of the O–H(δ^+) bonds is faster by orders of magnitude than the subsequent hydrogen addition to the quinoline molecules. Therefore, the interaction between the PtNPs and quinoline, which is size-dependent, becomes critical to the overall reaction rate, and accounts for the observed size-dependence in the catalysis. By combining the above results, a mechanism of the size-dependent catalysis can be proposed as follows (Figure 4e). First, H_2 is activated on the Pt surface, forming O–H(δ^+) and Pt–H(δ^-) species. Meanwhile, quinoline is chemisorbed on the surface of PtNPs adopting a tilted configuration with decreased electron density. For PtNPs of small sizes, the enhanced interaction and electron transfer facilitates the hydrogen transfer from H(δ^-)/H(δ^+) pairs to the quinoline molecules.[52,53] However, if the PtNPs are extremely small, the interaction between PtNPs and H_2/quinoline becomes too strong, which leads to poisoning of the catalyst and thus low reaction rates. The volcano-shaped dependence of the catalytic activity on the size of the PtNPs is thus rationalized.

In summary, we have revealed a strong size effect of PtNPs on their catalytic activity in the regioselective hydrogenation reactions of quinoline. The size effect has been largely attributed to the size-dependent d-band electron structure of the PtNPs and thus their interaction with the reactants. The size effect and the synthesis strategy reported herein are extendable to many other metals (an example see Figure S15) and reactions, and therefore provide a general methodology for harnessing the catalytic activity of metal-nanoparticle-based catalysts, opening up great opportunities in the design of catalysts for a broad range of organic syntheses, especially for those requiring harsh conditions (Table S4, Figure S8).

Acknowledgements

C.G. thanks the support from the National Natural Science Foundation of China (21301138, 21671156). Q.C. acknowledges support from the China Postdoctoral Science Foundation (2015M582634). Y.Y. (Yin) acknowledges the support from U.S. Department of Energy (DE-SC0002247). J.G. acknowledges the technical support from Matthew Marcus on BL10.3.2 at the Advanced Light Source (ALS). The ALS is supported by the U.S. Department of Energy (DE-AC02-05CH11231). Y.Y. (Ye) thanks the support of an ALS Doctoral Fellowship. We thank K. Ren at the Research Institute of Petroleum Processing for assistance with DFT calculations.

Keywords: d-band electron structure · heterogeneous catalysis · hydrogenation reactions · platinum nanoparticles · size effects

How to cite: *Angew. Chem. Int. Ed.* **2016**, *55*, 15656–15661
Angew. Chem. **2016**, *128*, 15885–15890

[1] M. Haruta, T. Kobayashi, H. Sano, N. Yamada, *Chem. Lett.* **1987**, *16*, 405–408.
[2] M. Valden, X. Lai, D. W. Goodman, *Science* **1998**, *281*, 1647–1650.
[3] K. Ding, A. Gulec, A. M. Johnson, N. M. Schweitzer, G. D. Stucky, L. D. Marks, P. C. Stair, *Science* **2015**, *350*, 189–192.
[4] K. Yamamoto, T. Imaoka, W. J. Chun, O. Enoki, H. Katoh, M. Takenaga, A. Sonoi, *Nat. Chem.* **2009**, *1*, 397–402.
[5] E. Toyoda, R. Jinnouchi, T. Hatanaka, Y. Morimoto, K. Mitsuhara, A. Visikovskiy, Y. Kido, *J. Phys. Chem. C* **2011**, *115*, 21236–21240.
[6] F. J. Perez-Alonso, D. N. McCarthy, A. Nierhoff, P. Hernandez-Fernandez, C. Strebel, I. E. Stephens, J. H. Nielsen, I. Chorkendorff, *Angew. Chem. Int. Ed.* **2012**, *51*, 4641–4643; *Angew. Chem.* **2012**, *124*, 4719–4721.
[7] T. Imaoka, H. Kitazawa, W. J. Chun, S. Omura, K. Albrecht, K. Yamamoto, *J. Am. Chem. Soc.* **2013**, *135*, 13089–13095.
[8] T. Imaoka, H. Kitazawa, W. J. Chun, K. Yamamoto, *Angew. Chem. Int. Ed.* **2015**, *54*, 9810–9815; *Angew. Chem.* **2015**, *127*, 9948–9953.
[9] L. Huang, B. Han, Y. Xi, R. C. Forrey, H. Cheng, *ACS Catal.* **2015**, *5*, 4592–4597.
[10] H. Wang, Y. Wang, Z. Zhu, A. Sapi, K. An, G. Kennedy, W. D. Michalak, G. A. Somorjai, *Nano Lett.* **2013**, *13*, 2976–2979.
[11] A. Corma, P. Concepcion, M. Boronat, M. J. Sabater, J. Navas, M. J. Yacaman, E. Larios, A. Posadas, M. A. Lopez-Quintela, D. Buceta, E. Mendoza, G. Guilera, A. Mayoral, *Nat. Chem.* **2013**, *5*, 775–781.
[12] H. Wei, X. Liu, A. Wang, L. Zhang, B. Qiao, X. Yang, Y. Huang, S. Miao, J. Liu, T. Zhang, *Nat. Commun.* **2014**, *5*, 5634.
[13] W. Huang, J. N. Kuhn, C.-K. Tsung, Y. Zhang, S. E. Habas, P. Yang, G. A. Somorjai, *Nano Lett.* **2008**, *8*, 2027–2034.
[14] G. A. Somorjai, J. Y. Park, *Angew. Chem. Int. Ed.* **2008**, *47*, 9212–9228; *Angew. Chem.* **2008**, *120*, 9352–9368.
[15] L. Chen, J. Hu, R. Richards, *J. Am. Chem. Soc.* **2009**, *131*, 914–915.
[16] C. Xiao, R. V. Maligal-Ganesh, T. Li, Z. Qi, Z. Guo, K. T. Brashler, S. Goes, X. Li, T. W. Goh, R. E. Winans, W. Huang, *ChemSusChem* **2013**, *6*, 1915–1922.
[17] T. Zhang, H. Zhao, S. He, K. Liu, H. Liu, Y. Yin, C. Gao, *ACS Nano* **2014**, *8*, 7297–7304.
[18] L. Shang, T. Bian, B. Zhang, D. Zhang, L.-Z. Wu, C.-H. Tung, Y. Yin, T. Zhang, *Angew. Chem. Int. Ed.* **2014**, *53*, 250–254; *Angew. Chem.* **2014**, *126*, 254–258.
[19] Y. Pei, C. Xiao, T.-W. Goh, Q. Zhang, S. Goes, W. Sun, W. Huang, *Surf. Sci.* **2016**, *648*, 299–306.
[20] D. Ge, L. Hu, J. Wang, X. Li, F. Qi, J. Lu, X. Cao, H. Gu, *ChemCatChem* **2013**, *5*, 2183–2186.
[21] D. Ren, L. He, L. Yu, R. S. Ding, Y. M. Liu, Y. Cao, H. Y. He, K. N. Fan, *J. Am. Chem. Soc.* **2012**, *134*, 17592–17598.
[22] A. R. Katritzky, S. Rachwal, B. Rachwal, *Tetrahedron* **1996**, *52*, 15031–15070.
[23] G. E. Dobereiner, A. Nova, N. D. Schley, N. Hazari, S. J. Miller, O. Eisenstein, R. H. Crabtree, *J. Am. Chem. Soc.* **2011**, *133*, 7547–7562.
[24] R. H. Fish, A. D. Thormodsen, G. A. Cremer, *J. Am. Chem. Soc.* **1982**, *104*, 5234–5237.
[25] W.-B. Wang, S.-M. Lu, P.-Y. Yang, X.-W. Han, Y.-G. Zhou, *J. Am. Chem. Soc.* **2003**, *125*, 10536–10537.
[26] R. Yamaguchi, C. Ikeda, Y. Takahashi, K.-i. Fujita, *J. Am. Chem. Soc.* **2009**, *131*, 8410–8412.
[27] K. Okamoto, R. Akiyama, H. Yoshida, T. Yoshida, S. Kobayashi, *J. Am. Chem. Soc.* **2005**, *127*, 2125–2135.
[28] Y. Gong, P. Zhang, X. Xu, Y. Li, H. Li, Y. Wang, *J. Catal.* **2013**, *297*, 272–280.
[29] Y. Zhu, F. Zaera, *Catal. Sci. Technol.* **2014**, *4*, 955–962.
[30] A. K. Prashar, S. Mayadevi, R. Nandini Devi, *Catal. Commun.* **2012**, *28*, 42–46.
[31] M. Dhiman, V. Polshettiwar, *J. Mater. Chem. A* **2016**, *4*, 12416–12424.
[32] J. N. Kuhn, W. Huang, C.-K. Tsung, Y. Zhang, G. A. Somorjai, *J. Am. Chem. Soc.* **2008**, *130*, 14026–14027.
[33] C.-K. Tsung, J. N. Kuhn, W. Huang, C. Aliaga, L.-I. Hung, G. A. Somorjai, P. Yang, *J. Am. Chem. Soc.* **2009**, *131*, 5816–5822.
[34] V. V. Pushkarev, N. Musselwhite, K. An, S. Alayoglu, G. A. Somorjai, *Nano Lett.* **2012**, *12*, 5196–5201.
[35] J. Liu, S. Z. Qiao, H. Liu, J. Chen, A. Orpe, D. Zhao, G. Q. Lu, *Angew. Chem. Int. Ed.* **2011**, *50*, 5947–5951; *Angew. Chem.* **2011**, *123*, 6069–6073.
[36] N. Li, Q. Zhang, J. Liu, J. Joo, A. Lee, Y. Gan, Y. Yin, *Chem. Commun.* **2013**, *49*, 5135–5137.
[37] Y. Sun, L. Zhuang, J. Lu, X. Hong, P. Liu, *J. Am. Chem. Soc.* **2007**, *129*, 15465–15467.
[38] Y. Borodko, P. Ercius, V. Pushkarev, C. Thompson, G. Somorjai, *J. Phys. Chem. Lett.* **2012**, *3*, 236–241.
[39] M. J. Hossain, H. Tsunoyama, M. Yamauchi, N. Ichikuni, T. Tsukuda, *Catal. Today* **2012**, *183*, 101–107.
[40] S. Mukerjee, S. Srinivasan, M. P. Soriaga, J. McBreen, *J. Electrochem. Soc.* **1995**, *142*, 1409–1422.
[41] J. Xing, J. F. Chen, Y. H. Li, W. T. Yuan, Y. Zhou, L. R. Zheng, H. F. Wang, P. Hu, Y. Wang, H. J. Zhao, Y. Wang, H. G. Yang, *Chem. Eur. J.* **2014**, *20*, 2138–2144.
[42] P. D. C. King, T. D. Veal, A. Schleife, J. Zúñiga-Pérez, B. Martel, P. H. Jefferson, F. Fuchs, V. Muñoz-Sanjosé, F. Bechstedt, C. F. McConville, *Phys. Rev. B* **2009**, *79*, 205205.
[43] T. Hofmann, T. H. Yu, M. Folse, L. Weinhardt, M. Bär, Y. Zhang, B. V. Merinov, D. J. Myers, W. A. Goddard, C. Heske, *J. Phys. Chem. C* **2012**, *116*, 24016–24026.
[44] B. Hammer, J. K. Nørskov, *Nature* **1995**, *376*, 238–240.
[45] B. Hammer, Y. Morikawa, J. K. Nørskov, *Phys. Rev. Lett.* **1996**, *76*, 2141–2144.
[46] V. Stamenkovic, B. S. Mun, K. J. Mayrhofer, P. N. Ross, N. M. Markovic, J. Rossmeisl, J. Greeley, J. K. Norskov, *Angew. Chem. Int. Ed.* **2006**, *45*, 2897–2901; *Angew. Chem.* **2006**, *118*, 2963–2967.
[47] B.-S. Choi, S. M. Kim, J. Gong, Y. W. Lee, S. W. Kang, H.-S. Lee, J. Y. Park, S. W. Han, *Chem. Eur. J.* **2014**, *20*, 11669–11674.

[48] T. Bligaard, J. K. Nørskov, S. Dahl, J. Matthiesen, C. H. Christensen, J. Sehested, *J. Catal.* **2004**, *224*, 206 – 217.
[49] Z. Hens, J. C. Martins, *Chem. Mater.* **2013**, *25*, 1211 – 1221.
[50] P. Liu, Y. Zhao, R. Qin, S. Mo, G. Chen, L. Gu, D. M. Chevrier, P. Zhang, Q. Guo, D. Zang, B. Wu, G. Fu, N. Zheng, *Science* **2016**, *352*, 797 – 800.
[51] J. T. Miller, B. L. Meyers, F. S. Modica, G. S. Lane, M. Vaarkamp, D. C. Koningsberger, *J. Catal.* **1993**, *143*, 395 – 408.
[52] R. Noyori, T. Ohkuma, *Angew. Chem. Int. Ed.* **2001**, *40*, 40 – 73; *Angew. Chem.* **2001**, *113*, 40 – 75.
[53] R. M. Bullock, *Chem. Eur. J.* **2004**, *10*, 2366 – 2374.

Manuscript received: October 3, 2016
Final Article published: November 11, 2016

